Title	Use of n-type amorphous silicon films as an electron transport layer in the perovskite solar cells
Author(s)	Song, Zhancheng; Sumai, Yuuka; HUYNH, Tu Thi Cam; Md. Shahiduzzaman; Taima, Tetsuya; Ohdaira, Keisuke
Citation	Japanese Journal of Applied Physics, 61(SB): SB1012-1-SB1012-4
Issue Date	2022-01-25
Type	Journal Article
Text version	author
URL	http://hdl.handle.net/10119/18177
Rights	This is the author's version of the work. It is posted here by permission of The Japan Society of Applied Physics. Copyright (C)2022 The Japan Society of Applied Physics. Zhancheng Song, Yuuka Sumai, Huynh Thi Cam Tu, Md. Shahiduzzaman , Tetsuya Taima and Keisuke Ohdaira , Japanese Journal of Applied Physics, 61(SB), 2022, SB1012-1-SB1012-4. https://doi.org/10.35848/1347-4065/ac2c99
Description	

Use of n-type amorphous silicon films as an electron transport layer in the perovskite solar cells

Zhancheng Song[1], Yuuka Sumai[2], Huynh Thi Cam Tu[1], Md. Shahiduzzaman[2], Tetsuya Taima[2,3*], Keisuke Ohdaira[1*]

[1]Japan Advanced Institute of Science and Technology, Asahidai, Nomi, Ishikawa 923-1292, Japan

[2]Graduate School of Frontier Science Initiative, Kanazawa University, Kakuma, Kanazawa 920-1192, Japan

[3]Nanomaterials Research Institute, Kanazawa University, Kakuma, Kanazawa, 920-1192, Japan

*E-mail: taima@se.kanazawa-u.ac.jp; ohdaira@jaist.ac.jp

We have investigated the use of n-type amorphous silicon (n-a-Si) films as the electron transport layers (ETL) in perovskite (PVK) solar cells, aiming at the application to PVK/Si tandem solar cells. The use of n-a-Si as the ETL in MAPbI$_3$ PVK solar cells was attempted, and the power conversion efficiency (PCE) of fluorine-doped tin oxide- (FTO-) based solar cells was improved due to an improvement in coverage on FTO with thicker n-a-Si, but the external quantum efficiency in the short wavelength region was decreased due to parasitic absorption of n-a-Si. The use of indium tin oxide with a flat surface resulted in a PCE of 1.25% for the solar cells with 10-nm-thick n-a-Si. This work indicates that n-a-Si is a potential ETL candidate for PVK solar cells and provides strategic guidance for the future vacuum-integrated process of PVK/Si heterojunction tandem solar cells, which can be feasible for efficient mass production.

I. Introduction

The power conversion efficiency (PCE) of Si heterojunction (SHJ) solar cells using single crystal silicon (c-Si) and amorphous silicon (a-Si) is 26.7%,[1-6] which is close to the theoretical efficiency limit of c-Si solar cell (29.4%).[2] Due to the small bandgap (~1.12 eV) of c-Si absorber, the part of photon energies larger than c-Si bandgap is converted to thermal energy instead of electrical energy, which causes a thermalization loss.[7] A tandem solar cell with a top cell consisting of a wider bandgap material on a c-Si bottom cell can reduce the thermalization loss. Perovskite (PVK) materials with advantages of high absorption coefficient, long diffusion length, low excitation energy, and tunable bandgap (1.18–2.3 eV) could be a promising candidate for the top cell material of the tandem solar cell with a PCE of >30%.[8-19]

So far, most of PVK solar cells have been fabricated with a TiO_2 film as an electron transport layer (ETL). However, thermal annealing of TiO_2 of >450 °C[20-21] may degrade the passivation quality of a-Si on a c-Si surface in the SHJ bottom cell with a thermal tolerance of ~200 °C, resulting in a reduction of open-circuit voltage (V_{oc}).[22] Moreover, the disadvantages of TiO_2 ETL such as solution-based coating method as well as having a property of high sensitivity against ultra-violet illumination[23] lead to difficulties in the fabrication of large-area and stable tandem solar cells. Additionally, a commonly used TiO_2 film as the n-type ETL in PVK cells comprises the drawbacks, including the low conductivity and electron mobility, which are unfavorable for efficient electron collection and transport.[24] Therefore, the development of ETL materials is highly required for developing the PVK solar cell industry.

In this study, we have investigated the n-type a-Si (n-a-Si) formed by catalytic chemical vapor deposition (Cat-CVD), and used it as the ETL in the PVK cell. Cat-CVD n-a-Si with a bandgap of 1.7–1.8 eV, low thermal budget process (~250 °C), and less sensitive to illumination due to low hydrogen concentration[25] is expected to obtain high-performance and high-stability PVK/SHJ tandem solar cells. Furthermore, the study of PVK cells with Cat-CVD n-a-Si ETL will provide guiding information to the vacuum-integrated process of PVK/SHJ tandem solar cells, which is feasible for mass production.

We report our initial results on the characterization of the PVK cells with Cat-CVD n-a-Si as ETL and $MAPbI_3$ as absorber. We particularly present the effect of n-a-Si thickness as well as substrate morphology on the resultant PVK cells performance.

2. Experimental methods

2.1 Deposition of Cat-CVD n-a-Si

n-a-Si films were formed by Cat-CVD, in which precursor gases of silane (SiH_4), phosphine (PH_3) and hydrogen (H_2) were introduced into a vacuum chamber at a gas pressure (P_g) of 2 Pa, and then decomposed by reacting with a tungsten catalyzing wire heated at 1800 °C and subsequent gas-phase reactions.[26-28] Substrate temperature during the deposition of n-a-Si films was set at 250 °C, while deposition durations were varied from 8 to 300 s to obtain n-a-Si films with thicknesses of 5–100 nm. The flow rates (FR) of SiH_4, H_2, and PH_3 gases were fixed at 20, 50, and 1.53 sccm, respectively. The conductivity of the n-a-Si films was ~2E−3 S/cm.

2.2 Fabrication of PVK cells with Cat-CVD n-a-Si ETL

Figure 1 shows the cross-sectional schematic of a planar PVK cell with Cat-CVD n-a-Si as ETL. n-a-Si films with thicknesses from 5 to 100 nm were deposited on glass substrates coated by FTO or ITO as a transparent electrode. The $MAPbI_3$ solution, which was synthesized by dissolving 1 M PbI_2 and 1 M CH_3NH_3I in DMF:DMSO (1:4) mixed solvent and stirring at 70 °C for 60 min, was then spin-coated on the n-a-Si using antisolvent technique (chlorobenzene solution) and then heated on a hotplate at 100 °C for 60 min. Thickness of the $MAPbI_3$ film was ~300 nm, and their optical bandgap was estimated to be ~1.6 eV from their optical transmittance spectra (not shown). Finally, a 250-nm-thick spiro-OMeTAD hole transport layer (HTL) and 100-nm-thick gold (Au) electrodes were sequentially deposited on $MAPbI_3$ film by spin-coating and thermal evaporation, respectively. A PVK solar cell with a TiO_2 ETL was also fabricated as a reference cell. The details for the formation process of $MAPbI_3$, spiro-OMeTAD and TiO_2 can be referred elsewhere.[20, 21, 29]

2.3 Characterization

Surface morphology and cross-section of the PVK cell were observed by field emission scanning electron microscopy (SEM) (S-4800, Hitachi High-Tech). The current density–voltage (J–V) curves were obtained by measuring the cells under one-sun light with an active area of 0.09 cm^2. The external quantum efficiency (EQE) of the cells was evaluated using a monochromatic xenon arc light system (SMI-250JA, Bunkoukeiki).

3

3. Results and discussion

Figure 2 shows the current–voltage (I–V) characteristics of the devices with a structure of Al/n-a-Si/FTO/Al, in which the thickness of n-a-Si films was varied from 5 to 100 nm. Linear I–V curves are obtained for all the devices. This indicates that Ohmic contact was formed at the n-a-Si/FTO interface at a deposition temperature of 250 °C, without an additional annealing process. It should be noted that I–V characteristics of the devices with the n-a-Si films with thicknesses of 5 to 50 nm are similar to one of the devices without n-a-Si film. Therefore we assumed that there were leakage currents due to a direct contact between Al and FTO electrodes. This issue will be discussed later. In addition, we also confirmed an Ohmic contact between n-a-Si and ITO.

Figure 3 shows J–V characteristics of the solar cells with n-a-Si and TiO_2 on FTO, and 10-nm-thick n-a-Si on ITO electrodes with forward and reverse bias scans. We fabricated and measured ten cells for each condition, and the best performance cell was plotted. Performance parameters of the solar cells were summarized in Table I. For all the cells, higher efficiency was obtained during the reverse direction scanning, while the efficiency decreased during the forward direction scanning. The large hysteresis seen in the J–V curve of the PVK solar cells might be attributed to the presence of trap defects, caused by the excess ions and the grain size of PVK, at and near the interface between PVK and carrier transport layers.[30,31] In the case of the reference cell with TiO_2 as ETL, it has been confirmed that by improving interface quality of PVK and carrier transport layers the hysteresis could be significantly reduced, and the PCE could be increased to 18.43%.[29]

When n-a-Si was used as the ETL, performance of the cells with FTO electrode was improved by increasing thickness of the n-a-Si film. As the thickness of the n-a-Si film increased from 5 nm to 100 nm, the J_{sc} in the reverse scan increased from 0.049 to 4.2 mA/cm^2 and V_{oc} from 0.35 to 0.92 V. As a result, PCE increased from 0.0040 to 1.16%. On the other hand, the cell with 10-nm-thick n-a-Si on an ITO electrode showed the highest PCE of 1.25% in the reverse scan, which was better than the cell with 100-nm-thick n-a-Si on FTO electrode.

Figure 4(a) shows the cross-sectional SEM image of the cell with 50-nm-thick n-a-Si on FTO electrode. n-a-Si could not fully cover the rough surface of FTO, and there are direct contacts between the $MAPbI_3$ and FTO (see diagrams in Fig. 4(d)). On the other hand, in the sample with TiO_2 coating on FTO shown in Fig. 4(b), the direct contact

between MAPbI$_3$ and FTO is not observed, because the thickness of the film is about 200 nm and the TiO$_2$ precursor solution could easily spread on the rough FTO surface. In the case of incomplete coverage, direct contact between MAPbI$_3$ and FTO is expected to result in lower V_{oc}, J_{sc}, and FF. In other words, it is expected that the coverage is improved by increasing the thickness of n-a-Si, and the power generation performance is significantly improved. On the other hand, the use of thicker n-a-Si increases the series resistance and parasitic absorption,[32-35] and further improvement of efficiency is difficult on the structure with large roughness. The cross-sectional SEM image of the solar cell with ITO shown in Fig. 4(c) shows that on the ITO electrode with a flat surface, even n-a-Si films with a thickness of 10 nm can be formed with good coverage, and the efficiency is considered to be equivalent to that of the cell with 100-nm-thick n-a-Si on FTO.

Figure 5 shows the EQE spectra of MAPbI$_3$ solar cells fabricated with 10-nm-thick n-a-Si on ITO and 50-nm- and 100-nm-thick n-a-Si on FTO as ETL. In both spectra, the absorption edge is found around 800 nm, which is consistent with the estimated bandgap energy of ~1.6 eV. The EQE in the short wavelength region below 600 nm is reduced in the cell with FTO electrode. This is thought to be due to parasitic absorption in the thick a-Si film. [32-35] On the other hand, the cell with the flat ITO electrode has sufficient coverage even with 10-nm-thick n-a-Si, which leads to less parasitic absorption and resulting improvement in the EQE in the short wavelength region.

One of the reasons of the cells fabricated using n-a-Si films with sufficient coverage and Ohmic contact with ITO but have lower PCE than the cells with TiO$_2$ as ETL is explained using the band diagram shown in Fig. 6, which is based on the literature. [36] The conduction band minimum (CBM) levels of n-a-Si and TiO$_2$ are –4.0 eV and –4.1 eV, respectively. [36-38] Both materials are about 0.1–0.2 eV lower than the CBM of MAPbI$_3$ and electrons can be easily injected from MAPbI$_3$, enabling them to function as ETL. On the other hand, the valence band maximum (VBM) position of n-a-Si is only 0.3 eV lower than the VBM level of MAPbI$_3$, and the hole blocking effect is expected to be weak. We believe this is the reason for the lower J_{sc} and V_{oc}.

However, our simulation results with the AFORS-HET simulation tool, which will be published elsewhere, show that PCE of the cells with n-a-Si as ETL is more than 12 % at carrier concentration as low as 2.5×10^{14} cm^{-3} and defect density as high as 10^{20} cm^{-3}. Therefore, other reasons for obtaining the low PCE of the cell with n-a-Si should be

considered, such as the poor interface between n-a-Si and MAPbI$_3$. How to improve the efficiency of the PVK cell is currently under investigation.

4 Conclusions

MAPbI$_3$ based PVK solar cells with n-a-Si as the ETL are fabricated and evaluated. The performance of the cells with FTO electrodes improves with increasing n-a-Si thickness due to the improvement of the coverage of the rough surface of the FTO. In the case of ITO electrodes formed on flat glass substrates, the surface of ITO can be fully covered even with 10-nm-thick n-a-Si. As a result, the highest PCE of 1.25% could be achieved. The use of n-a-Si with an E_g of 1.8 eV results in large parasitic absorption and insufficient hole blocking. For further study, it is necessary to investigate how to widen the bandgap of n-a-Si to suppress the parasitic absorption and to enhance hole blocking.

Acknowledgment

References

1) K. Yamamoto, K. Yoshikawa, H. Uzu, and D. Adachi, Jpn. J. Appl. Phys. **57**, 08RB20 (2018).

2) K. Yoshikawa, H. Kawasaki, W. Yoshida, T. Irie, K. Konishi, K. Nakano, T. Uto, D. Adachi, M. Kanematsu, H. Uzu, and K. Yamamoto, Nature Energy **2,** 17032 (2017).

3) K. Yoshikawa, W. Yoshida, T. Irie, H. Kawasaki, K. Konishi K, H. Ishibashi, t. Asatani, D. Adachi, M. Kanematsu, H. Uzu and K. Yamamoto,   Sol. Energy Mater. Sol. Cells **173**, 37 (2017).

4) F. Sahli, J. Werner, B. A. Kamino, M. Bräuninger, R. Monnard, B. Paviet-Salomon, L. Barraud, L. Ding, J. J. Diaz Leon, D. Sacchetto, G. Cattaneo, M. Despeisse, M. Boccard, S. Nicolay, Q. Jeangros, B. Niesen, and C. Ballif, Nature Energy **17**, 820 (2018).

5) J. Werner, C-H Weng, A. Walter, L. Fesquet, J P Seif, S. De Wolf, B. Niesen, and C. Ballif, J. Phys. Chem. Lett **7**, 161 (2016)

6) A. Richter, M. Hermle, and S. W. Glunz, IEEE J. Photovoltaics **3**, 1184 (2013).

7) O. Dupré, R. Vaillon, M.A. Green, Sol Energy **140**, 73 (2016)

8) F. Hao, C. C. Stoumpos, D. H. Cao, R. P. H. Chang, and M. G. Kanatzidis, Nat. Photonics, **8**, 489 (2014)

9) S. D. Stranks, G. E. Eperon, G. Grancini, C. Menelaou, M. J. Alcocer, T. Leijtens, L. M. Herz, A. Petrozza and H. J. Snaith, Science, **342**, 341(2013).

10) G. Xing, N. Mathews, S. Sun, S. S. Lim, Y. M. Lam, M. Gratzel, S. Mhaisalkar and T. C. Sum, Science, **342**, 344 (2013).

11) A. Miyata, A. Mitioglu, P. Plochocka, O. Portugall, J. T. W. Wang, S. D. Stranks, H. J. Snaith and R. J. Nicholas, Nat. Phys., **11**, U582 (2015).

12) D.P. McMeekin, G. Sadoughi, W. Rehman, G. E. Eperon, M. Saliba, M. T. Horantner, A. Haghighirad, N. Sakai, L. Korte, B. Rech, M. B. Johnston, L. M. Herz and H. J. Snaith,   Science **351**, 151 (2016).

13) K. A .Bush, A. F. Palmstrom, Z. J. Yu, M. Boccard, R. Cheacharoen, J. P. Mailoa, D. P. McMeekin, R. L. Z. Hoye, C. D. Bailie, T. Leijtens, I. M. Peters, M. C. Minichetti, N. Rolston, R. Prasanna, S. Sofia, D. Harwood, W. Ma, F. Moghadam, H. J. Snaith, T. Buonassisi, Z. C. Holman, S. F. Bent, and M. D. McGehee, Nature Energy **2**, 17009 (2017).

14) Y. Ogomi, A. Morita, S. Tsukamoto, T. Saitho, N. Fujikawa, Q. Shen, T. Toyoda, K. Yoshino, S. S. Pandey, T. Ma and S. Hayase, J. Phys. Chem. Lett., **5**, 1004 (2014).

15) P. Löper, S.-J. Moon, S. Martín de Nicolas, B. Niesen, M. Ledinsky, S. Nicolay, J. Bailat, J.-H. Yum, S. De Wolf, C. Ballif, Phys. Chem. Chem. Phys., **17**, 1619 (2015).

16) Z. J. Yu, M. Leilaeioun, Z. Holman, Nat. Energy, **1**, 16137 (2016).

17) I. Almansouri, A. Ho-Baillie, and M. A. Green, Jpn. J. Appl. Phys. **54**, 08KD04 (2015).

18) Md. Shahiduzzaman, S. Fukaya, E. Y. Muslih, L. Wang, M. Nakano, Md. Akhtaruzzaman, M. Karakawa, K. Takahashi, J.-M. Nunzi, and T. Taima, Materials **13**, 2207 (2020).

19) Md. Shahiduzzaman, E. Y. Muslih, A.K. Mahmud Hasan, L.L. Wang, S. Fukaya, M. Nakano, M. Karakawa, K. Takahashi, Md. Akhtaruzzaman, J.-M. Nunzi, and T. Taima, Chem. Eng. J. **411**, 128461 (2021).

20) Md. Shahiduzzaman, D. Kuwahara, M.Nakano, M. Karakawa, K. Takahashi, L. Nunzi and T. Taima, Nanomaterials **10**, 1676 (2020).

21) Md. Shahiduzzaman, A. Kulkarni, S. Visal, L. L. Wang, M. Nakano, M. Karakawa, K. Takahashi, S. Umezu, A. Masuda, S. Iwamori, M. Isomura, T. Miyasaka, K.Tomita, and T. Taima, Sustain. Energy Fuels, **4**, 2009 (2020).

22) S. D. Wolf and M. Kondo, J. Appl. Phys. **105**, 103707 (2009).

23) T. Leijtens, G. E. Eperon, S. Pathak, A. Abate, M. M. Lee, and H. J. Snaith, Nat. Commun. **4**, 2885 (2013).

24) K. Mahmood, S. Sarwarb, and M. T. Mehranb, RSC Adv. **7**, 17044 (2017).

25) Y. Ishibashi, A. Masuda, and H. Matsumura, Thin Solid Films **395,** 138 (2001).

26) H. Umemoto, Chem. Vap. Deposition 16, 275 (2010).

27) S. Nakamura, K.Matsumoto, A.Susa, and M. Koshi, J. Non-Cryst. Solids **352**, 919 (2006).

28) H. Umemoto, Y. Nishihara, T. Ishikawa, and S. Yamamoto, Jpn. J. Appl. Phys. **51**, 086501 (2012).

29) L.L. Wang, Md. Shahiduzzaman, E. Y. Muslih, M. Nakano, M. Karakawa, K.Takahashi, K. Tomita, J. M. Nunzi, T. Taima, Nano Energy **86**, 106135 (2021).

30) H. J. Snaith, A. Abate, J. M. Ball, G. E. Eperon, T. Leijtens, N. K. Noel, S. D. Stranks, J. T.-W. Wang, K. Wojciechowski, and W. Zhang, J. Phys. Chem. Lett. **5,** 1511 (2014).

31) H.-S. Kim and N.-G. Park, J. Phys. Chem. Lett. **5,** 2927 (2014).

32) M. Taguchi, A. Yano, S. Tohoda, K. Matsuyama, Y. Nakamura, T. Nishiwaki, K. Fujita, and E. Maruyama, IEEE J. Photovoltaics **4**, 96 (2014).

33) T. C. Thi, K. Koyama, K. Ohdaira, and H. Matsumura, Sol. Energy Mater. Sol. Cells **100**, 169 (2012).

34) M. Tanaka, M. Taguchi, T. Matsuyama, T. Sawada, S. Tsuda, S. Nakano, H. Hanafusa, and Y. Kuwano, Jpn. J. Appl. Phys. **31**, 3518 (1992).

35) H. Fujiwara and M. Kondo, J. Appl. Phys. **101**, 054516 (2007).

36) S. Philip, O. T. Jan, A. C. Jeffrey, L. Igal, E. Eran, M. S. Erin, H. Gary, C. David and K. Antoin., ACS Appl. Mater. Interfaces **46**, 31491 (2016).

37) H. S. Jung and N.G. Park, Small. **11**, 10 (2015).

38) C. I. Ukah, R. V. Kruzelecky, D. Racansky, S. Zukotynski, and J. M. Perz, J. Non-Cryst. Solids **103**, 131 (1988).

Table I. Performance of PVK solar cells with Cat-CVD n-a-Si and TiO_2 as ETLs on FTO and ITO electrodes.

ETLs	TCO	Scan direction	PCE (%)	J_{sc} (mA/cm^2)	V_{oc} (V)	FF
200 nm TiO_2	FTO	Forward	10.47	19.92	0.86	0.61
		Reverse	13.23	19.95	0.95	0.69
5 nm n-a-Si	FTO	Forward	0.00	0.02	0.25	0.27
		Reverse	0.00	0.05	0.35	0.24
10 nm n-a-Si	FTO	Forward	0.03	0.24	0.42	0.29
		Reverse	0.06	0.45	0.49	0.25
50 nm n-a-Si	FTO	Forward	0.06	1.01	0.53	0.06
		Reverse	0.19	1.22	0.73	0.21
100 nm n-a-Si	FTO	Forward	0.52	4.46	0.69	0.17
		Reverse	1.16	4.17	0.92	0.30
10 nm n-a-Si	ITO	Forward	0.01	0.05	0.35	0.51
		Reverse	1.25	3.50	0.87	0.41

Figure Captions

Figure 1 (Color online) Schematic cross-sectional structure of a PVK solar cell with n-a-Si as an ETL.

Figure 2 (Color online) I–V characteristics of devices with a structure of Al/n-a-Si/FTO/Al, in which the thickness of n-a-Si varied from 5 to 100 nm. The inset shows the devices' structure.

Figure 3 (Color online) J–V characteristics of PVK solar cells with n-a-Si and TiO_2 on FTO, and 10-nm-thick n-a-Si on ITO electrodes with forward (dash line) and reverse bias (solid line) scans.

Figure 4 (Color online) Cross-sectional SEM images of PVK solar cells with (a) 50-nm-thick n-a-Si on FTO/textured glass, (b) 10-nm-thick n-a-Si on ITO/flat glass, (c) 200-nm-thick TiO_2 on FTO/textured glass, and (d) diagrams illustrating uncovered areas of FTO with 50-nm-thick n-a-Si, full covered ITO and FTO with 10-nm-thick n-a-Si and 200-nm-thick TiO_2, respectively.

Figure 5 (Color online) EQE spectra of the PVK solar cells with 50-nm- and 100-nm-thick n-a-Si on FTO, and 10-nm-thick n-a-Si on ITO electrodes.

Figure 6 (Color online) Band diagrams of (a) TiO_2/MAPbI$_3$/spiro-OMeTAD and (b) n-a-Si/MAPbI$_3$/spiro-OMeTAD
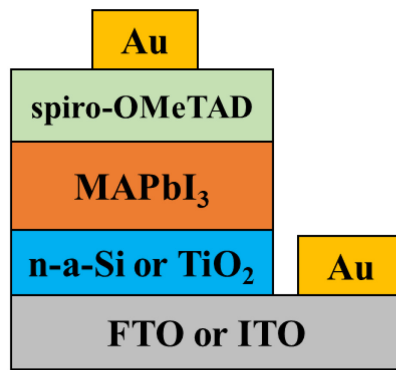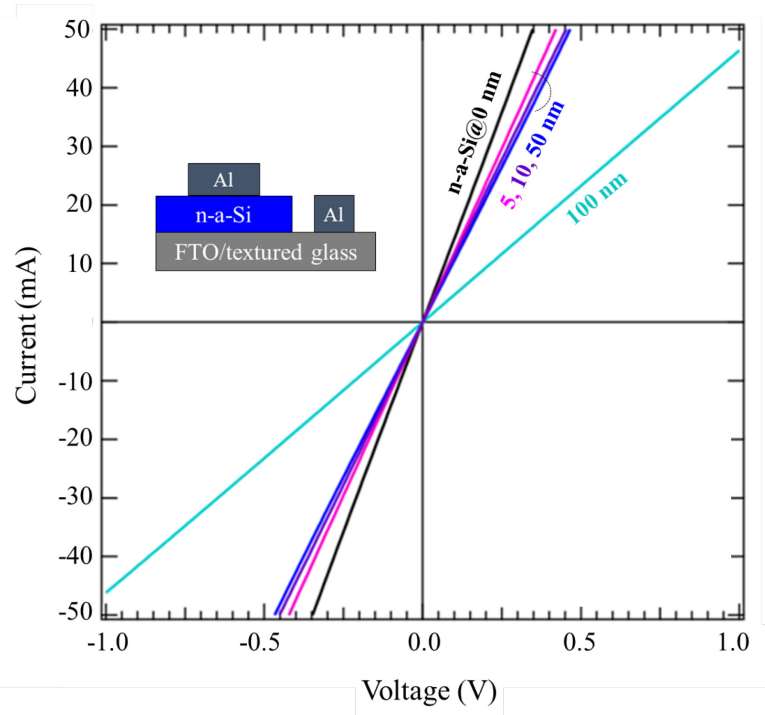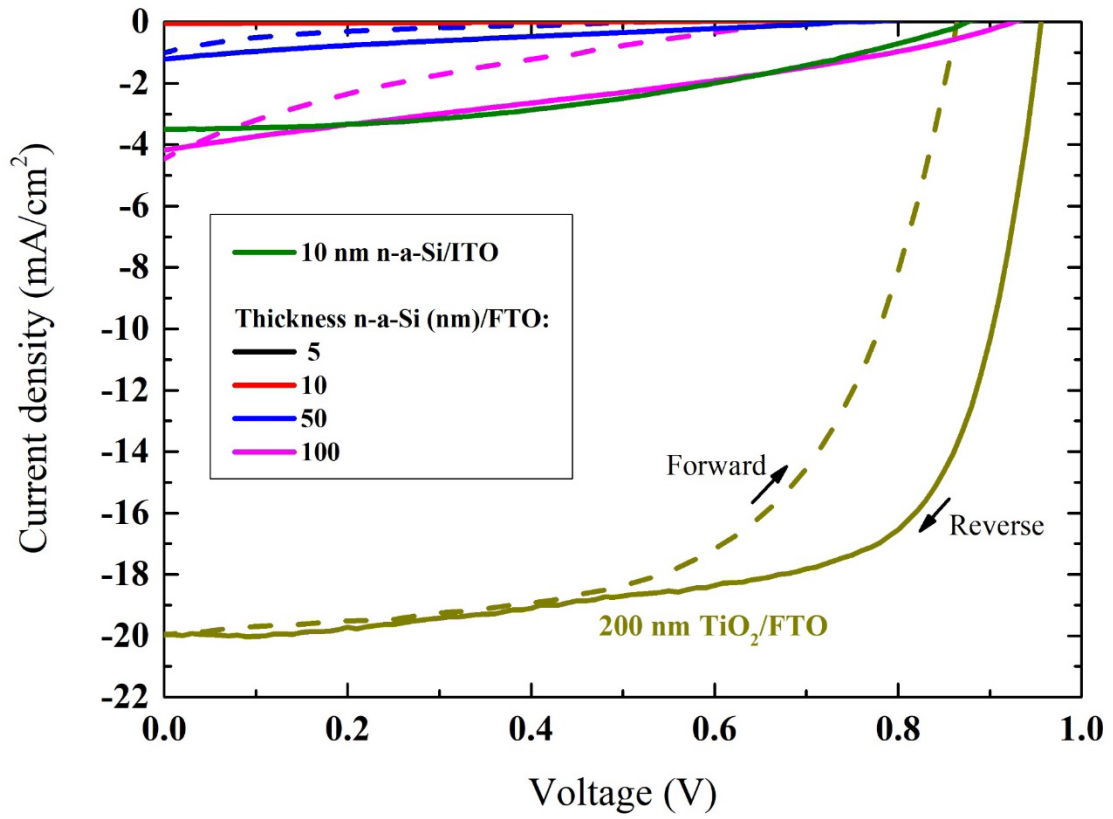
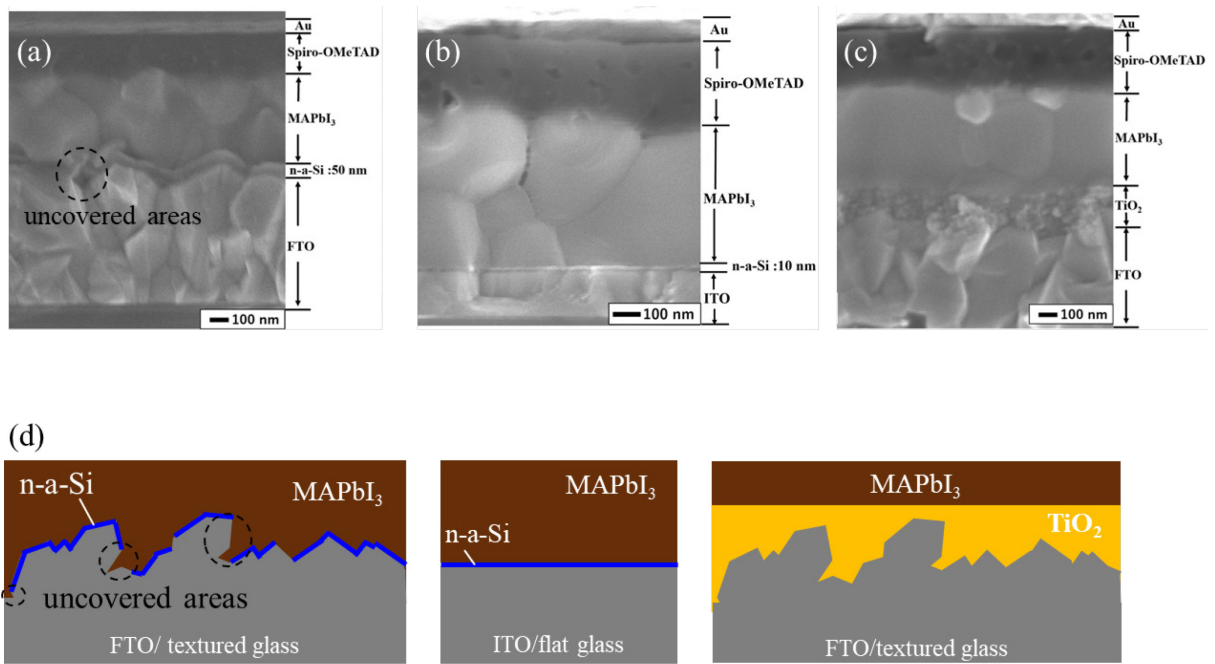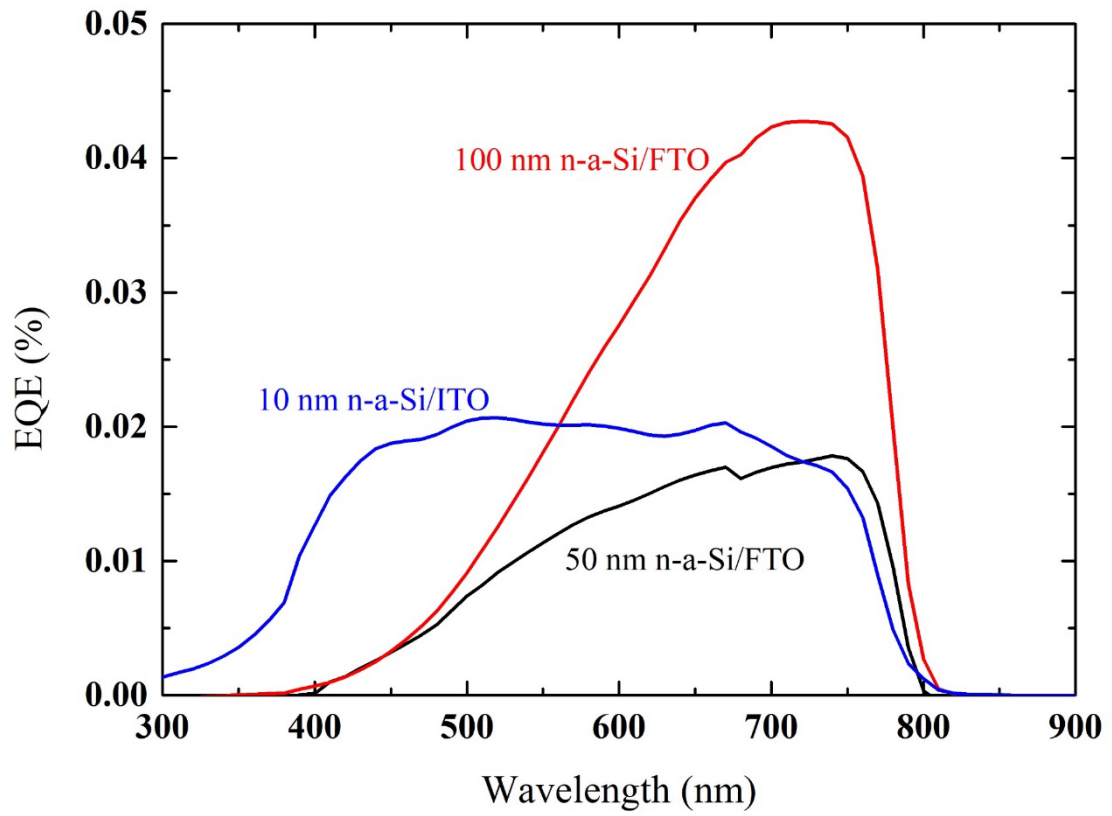Fig. 1. Song et al.

Fig. 2. Song et al.
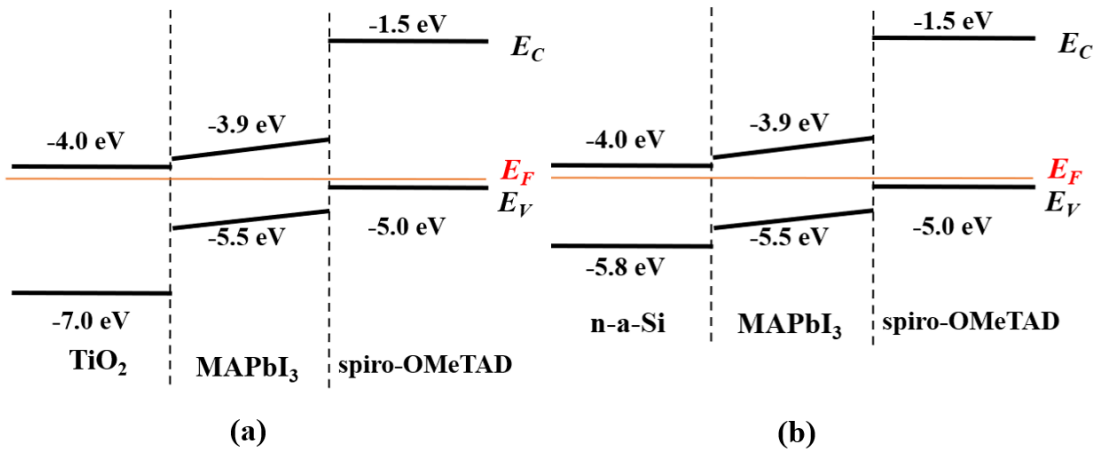
Fig. 3. Song et. al.

Fig. 4. Song et al.

Fig. 5. Song et al.

Fig. 6. Song et al.